

Location determining method of critical sliding surface of fillings in a karst cave of tunnel

P. Lin^{1a}, S.C. Li^{1b}, Z.H. Xu^{*1,2,3}, X. Huang^{1c}, D.D. Pang^{1d}, X.T. Wang^{1e} and J. Wang^{1f}

¹School of Qilu Transportation, Shandong University, Jinan, Shandong 250061, China

²Geotechnical & Structural Engineering Research Center, Shandong University, Jinan, Shandong 250061, China

³SinoProbe Center-China Deep Exploration Center, Chinese Academy of Geological Sciences, Beijing 100037, China

(Received June 4, 2018, Revised July 25, 2018, Accepted July 30, 2018)

Abstract. A location determining method is proposed for critical sliding surface in the stability analysis of the filling materials in karst caves. First, a preliminary location of the sliding surface is determined based on simulation results which includes displacement contour and plastic zone. The sliding surface will locate on the bottom contact interface when the friction angle is relative small. However, a weakened contact interface always becomes the critical sliding surface no matter what the friction angle is. Then when the friction angle becomes larger, the critical sliding surface inside fillings can be determined by a parabola, the coefficient of which increases linearly with the friction angle under the same cohesion. Finally, the critical sliding surface approximately remains unchanged with friction angle. The influence of cohesion is similar to that of friction angle. Although affected by shape, size or position of the karst cave, the critical sliding surface mainly depends on both friction angle and cohesion. Thus, this method is always useful in determining the critical sliding surface.

Keywords: critical sliding surface; stability analysis; filling materials; karst cave

1. Introduction

Tunnel construction easily suffers a serious water and mud inrush disaster in karst areas. Disaster often causes thousands of casualties, significant economic losses, adverse social impact and serious environmental damage. Water and mud inrush catastrophe is difficult to control, because the catastrophic evolution mechanism is extremely complex. A clear understanding of the mechanism is not yet formed. Hazard-causing structures include karst structure (such as karst caves, karst conduit etc.), fault fracture zone, intrusive contact structure etc. Resources of the disaster include water, solid filling materials (such as mylonite, cataclastite, soil etc.) and the mixture of water and solid materials. Water & mud-confining structure is consisting of the surrounding rock or the solid filling materials. Many

research achievements have been obtained regarding the mechanism for the failure of the surrounding rock since last century, such as the bending theory of beam and plate (Hoefsloot 2008, Barpi *et al.* 2011), the crack growth theory under hydraulic effect (Aliha *et al.* 2010, Damjanac *et al.* 2010, Carrier and Granet 2012), the key block theory etc. (Rutqvist *et al.* 2002). But less research is reported on the stability of the solid filling materials (Li *et al.* 2015, Serdar *et al.* 2015, Yang *et al.* 2015, Lin *et al.* 2016).

Stability of filling materials are conducted based on the slice method in the present study. The slice method is demonstrated highly efficient, simple and practical in stability analysis in slope and dam engineering field. Relevant theories and research achievements have been widely applied (Yamin and Liang 2010, Khosravi and Khabbazian 2012, Hajiazizi and Taviana 2013, Guerriero *et al.* 2014, Metya and Bhattacharya 2014, Mazaheri 2015, Gandomi *et al.* 2015). The slice method is superior to the numerical simulations or the model experiments in quickly analyzing the stability of the filling materials in karst caves. One thing to emphasize especially is that slopes or dams are restricted to a semi-space, but the filling materials in karst caves are restricted to a whole-space. In addition, the geological genesis, the hydrodynamic environment and the boundary conditions are more complicated in the whole-space analysis. Therefore, the previous achievements cannot be directly applied to the stability analysis of the filling materials in karst caves.

Location determining of critical sliding surface is the fundamental problem in the stability analysis of filling materials based on the slice method (Kahatadeniya *et al.* 2009, Khajehzadeh *et al.* 2011, 2012a, b, Gandomi *et al.* 2014, Kashani *et al.* 2016, Regmi and Jung 2016). Stability

*Corresponding author, Associate Professor

E-mail: zhenhao_xu@sdu.edu.cn

^aPh.D. Student

E-mail: sddxytlp@163.com

^bProfessor

E-mail: lishucai@sdu.edu.cn

^cPh.D. Student

E-mail: hx19891018@yeah.net

^dPh.D. Student

E-mail: pddyantu@163.com

^ePh.D. Student

E-mail: wangxintong0722@163.com

^fLecturer

E-mail: wjingsdu@163.com

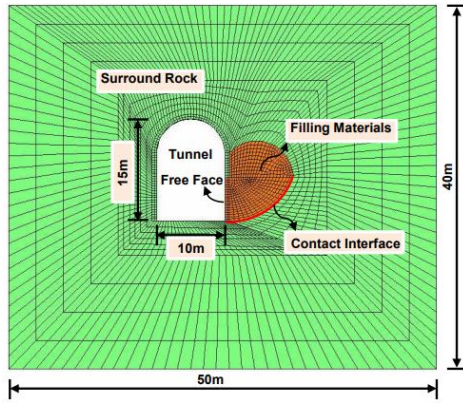


Fig. 1 Numerical simulation model

Table 1 Scenarios for preliminarily location of the critical sliding surface

Scenario	Filling Materials		Interface		
	φ ($^{\circ}$)	C (KPa)	State	φ ($^{\circ}$)	C (KPa)
I-1	18	2×10^4	not Weakened	18	2×10^4
I-2	32	2×10^4	not Weakened	32	2×10^4
I-3	32	2×10^4	Weakened	10	1×10^4
II-1	12	3×10^4	not Weakened	12	3×10^4
II-2	24	3×10^4	not Weakened	24	3×10^4
II-3	24	3×10^4	Weakened	10	1×10^4
III-1	8	4×10^4	not Weakened	8	4×10^4
III-2	14	4×10^4	not Weakened	14	4×10^4
III-3	14	4×10^4	Weakened	10	1×10^4

of filling materials with a soft interlayer is analyzed based on the transmit coefficient slice method or the Bishop method, where the weakened interface is simplified as the critical sliding surface (Li *et al.* 2015, Lin *et al.* 2016). However, critical sliding surface may appear inside fillings. In addition, the shape of a cave boundary is usually a straight line, a polyline, an arc, a curve or some other irregular shapes. Therefore, location determination of the critical sliding surface should be studied firstly.

A location determining method is proposed for critical sliding surface in stability analysis of filling materials in karst caves. Firstly, a preliminary location of the sliding surface is determined based on simulation results which includes displacement contour and plastic zone. Then an exact location is determined by a parabola method. The relationship between the coefficient of the parabola and friction angle is investigated and the influence of cohesion is discussed.

2. Numerical simulation scenarios

A numerical simulation model is established based on the FLAC3D software platform. This model is used to study the determination of critical sliding surface for filling materials in karst caves. The model is 40 m high and 50 m

Table 2 Scenarios for original sliding circle analysis

Scenario	Classification Basis	Subclass							
		1	2	3	4	5	6	7	8
IV	1	30	32	34	36	38	40	42	44
V	Cohesion (KPa)	24	26	28	30	32	34	36	38
VI		3	16	18	20	22	24	26	28
VII	4	8	10	12	14	16	18	20	22

wide. The height and width of the tunnel are 15 m and 10 m respectively. The revealed karst cave is filled. An interface is applied to define the contact interface between the surrounding rock and the filling materials. Detailed description of the model is shown in Fig. 1.

There are two conditions. Firstly, the interface between the surrounding rock and the filling materials is easier to be the critical sliding surface if the shear strength or the frictional resistance of the interface is reduced by the karst water corrosion and seepage. Secondly, the critical sliding surface may appear inside soils when the interface is not weakened.

Three scenarios are studied for the location pre-determining of the critical sliding surface, i.e., scenarios I, II and III with different cohesions of the filling materials. Each scenario is further divided into three scenarios. The first two scenarios are designed with different internal friction angles of the filling materials. The third scenario is designed with weakened interface. The cohesion and the friction angle of the weakened interface are smaller than that of the filling materials. Parameters of each scenario are listed as shown in Table 1.

Exact location of the critical sliding surface needs to be determined when the sliding surface appears inside the fillings. Thus, four scenarios are designed to study the determining method for the location of the critical sliding surface, i.e., scenarios IV, V, VI and VII with different cohesions of the filling materials. Each scenario is divided into several different scenarios with different friction angles of the filling materials. The cohesions or the internal friction angles of the filling materials for different scenarios are listed as shown in Table 2.

3. Results

3.1 Displacement analysis

Fig. 2 shows contour maps of displacement (larger than 20cm) under scenarios (a) I1 with $C = 2$ KPa and $\varphi = 18^{\circ}$, (b) I2 with $C = 2$ KPa and $\varphi = 32^{\circ}$, (c) I3 with $C = 2$ KPa, $\varphi = 32^{\circ}$ and a weakened interface, (d) II1 with $C = 3$ KPa and $\varphi = 12^{\circ}$, (e) II2 with $C = 3$ KPa and $\varphi = 24^{\circ}$, (f) II3 with $C = 3$ KPa, $\varphi = 24^{\circ}$ and a weakened interface, (g) III1 with $C = 4$ KPa and $\varphi = 8^{\circ}$, (h) III2 with $C = 4$ KPa and $\varphi = 14^{\circ}$, and (i) III3 with $C = 4$ KPa, $\varphi = 14^{\circ}$ and a weakened interface. Most displacement values are larger than 20 cm when the internal friction angle is relative small, such as scenarios I1, II1 and III1 in Fig. 2(a), 2(d) and 2(g), respectively, which indicates that wholesale collapse may occur in karst caves.

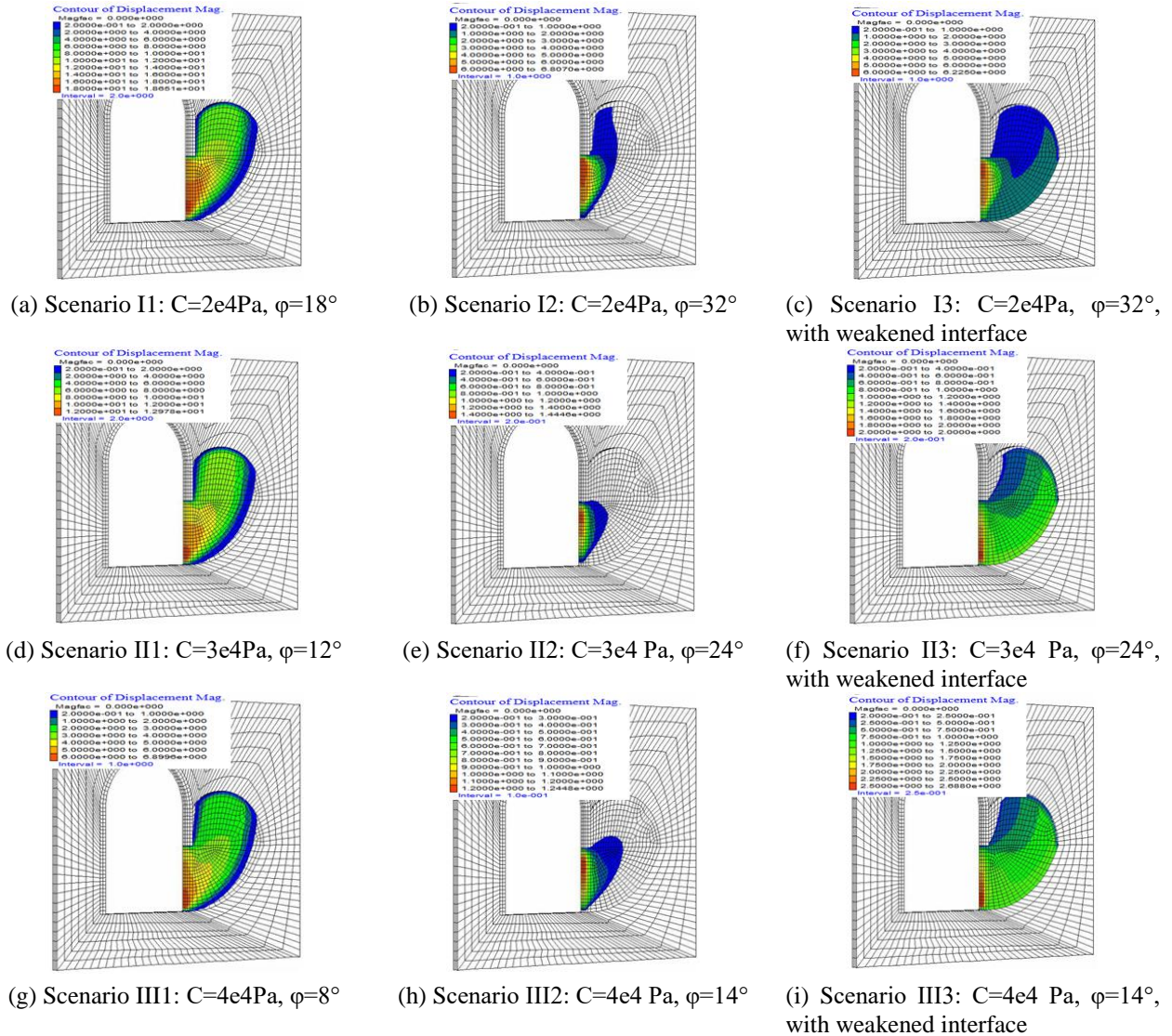


Fig. 2 Contour maps of displacement (larger than 20cm) under scenario #I, #II and #III

The failure surface may appear inside the fillings, because displacement values near the contact interface are much smaller than those inside the fillings. Only displacement values near the free face are larger than 20 cm when the internal friction angle becomes large, such as scenarios I2, II2 and III2 in Fig. 2(b), 2(e) and 2(h), respectively, which indicates that the fillings are stable. However, most displacement values become larger than 20cm with a weakened interface when the internal friction angle is still large, as shown in Fig. 2(c), 2(f) and 2(i). In addition, displacement values near the interface are larger than the values inside fillings. It is reasonable that the weakened contact interface is the critical failure surface.

3.2 Plastic state analysis

Fig. 3 shows plastic state under scenarios (a) IV2 with $C = 1\text{KPa}$ and $\varphi = 32^\circ$, (b) IV5 with $C = 1\text{KPa}$ and $\varphi = 38^\circ$, (c) IV8 with $C = 1\text{KPa}$ and $\varphi = 44^\circ$, (d) V2 with $C = 2\text{KPa}$ and $\varphi = 26^\circ$, (e) V5 with $C = 2\text{KPa}$ and $\varphi = 32^\circ$, (f) V8 with $C = 2\text{KPa}$ and $\varphi = 38^\circ$, (g) IV2 with $C = 3\text{KPa}$ and $\varphi = 18^\circ$,

(h) IV5 with $C = 3\text{KPa}$ and $\varphi = 24^\circ$, (i) IV8 with $C = 3\text{KPa}$ and $\varphi = 30^\circ$, (j) VI2 with $C = 4\text{KPa}$ and $\varphi = 10^\circ$, (k) VII5 with $C = 4\text{KPa}$ and $\varphi = 16^\circ$, and VIII8 with $C = 4\text{KPa}$ and $\varphi = 22^\circ$. Almost all elements become plastic state when the internal friction angle is relative small, such as scenarios IV2, V2, VI2 and VII2 in Fig. 3(a), 3(d), 3(g) and 3(j), respectively. Then the quantity of plastic element becomes small gradually with the internal friction angle, such as scenarios IV5, V5, VI5 and VII5 in Fig. 3(b), 3(e), 3(h) and 3(k), respectively. Only these elements near the free face become plastic state when the internal friction angle becomes large, such as scenarios IV8, V8, VI8 and VII8 in Fig. 3(c), 3(f), 3(i) and 3(l), respectively. These plastic elements are regarded as potential slip objects, and the bottom boundary of the plastic zone is regarded as the critical sliding surface. Seen from Fig. 3, the critical sliding surface becomes steeper with the internal friction angle or the cohesion. In addition, we found an interesting thing that when the internal friction angle becomes large, plastic zone extends up to the top of karst cave with a relative small cohesion, such as scenario IV8 in Fig. 3(c), but is confined

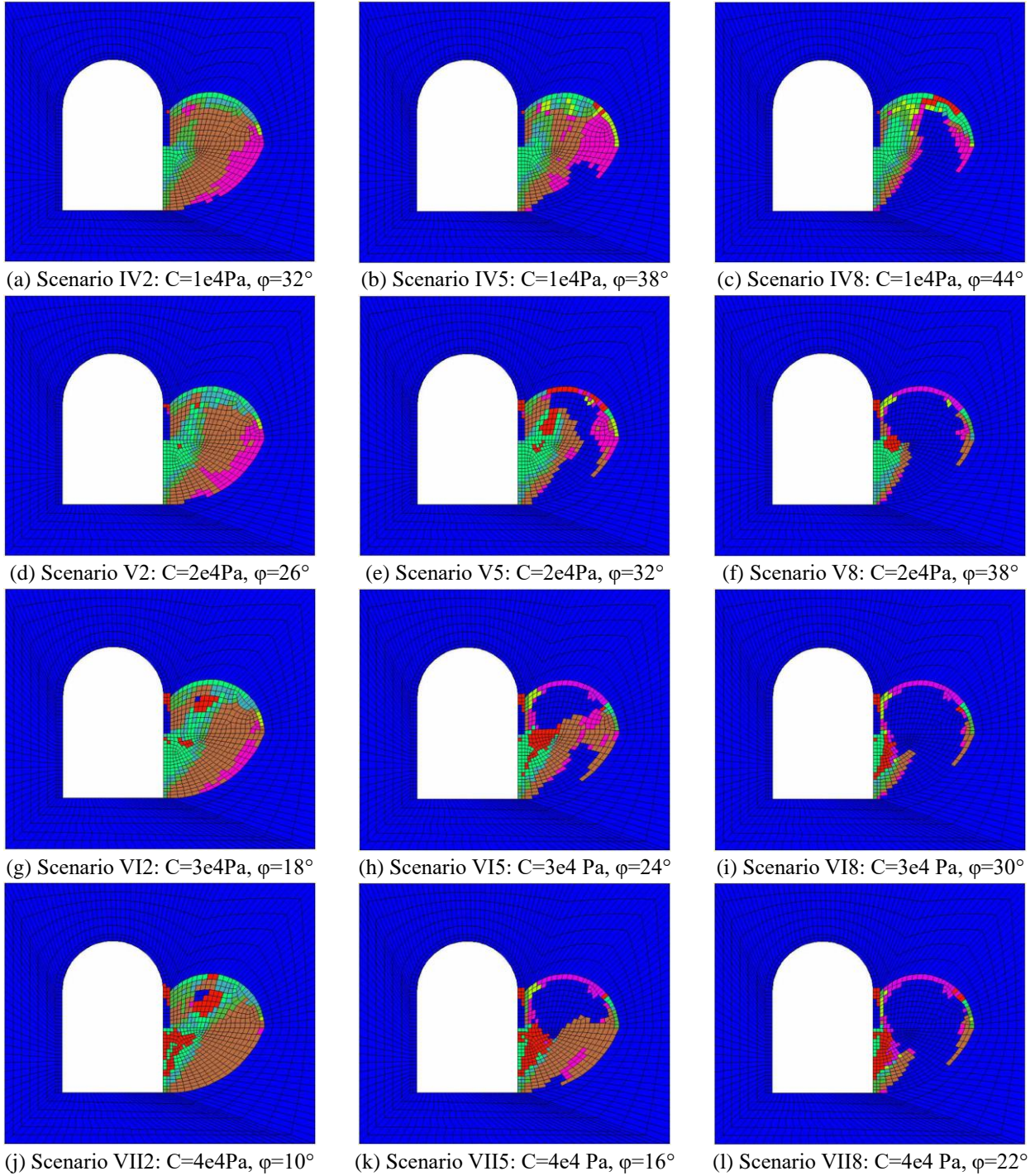


Fig. 3 Plastic state under scenario IV, V, VI and VII

Table 3 Preliminary location of the sliding surface

Cohesion C (KPa)	Friction angle φ ($^{\circ}$)	Sliding Location	Friction angle φ ($^{\circ}$)	Sliding Location	Friction angle φ ($^{\circ}$)	Sliding Location
1	$< 36^{\circ}$	Interface	$36^{\circ} \sim 44^{\circ}$	Inside fillings	$> 44^{\circ}$	Same as 44°
2	$< 32^{\circ}$	Interface	$32^{\circ} \sim 38^{\circ}$	Inside fillings	$> 38^{\circ}$	Same as 38°
3	$< 24^{\circ}$	Interface	$24^{\circ} \sim 30^{\circ}$	Inside fillings	$> 30^{\circ}$	Same as 30°
4	$< 18^{\circ}$	Interface	$18^{\circ} \sim 22^{\circ}$	Inside fillings	$> 22^{\circ}$	Same as 22°

to a small zone near the free face with a relative large cohesion, such as scenario V8 in Fig. 3(f).

3.3 Location pre-determining of the critical sliding surface

Based on simulation results, a preliminary location of the sliding surface is determined. When friction angle is smaller than 36° , 32° , 24° or 18° , the sliding surface locates on the bottom contact interface, when friction angle is in the range from $36^{\circ} \sim 44^{\circ}$, $32^{\circ} \sim 38^{\circ}$, $24^{\circ} \sim 30^{\circ}$ or $18^{\circ} \sim 22^{\circ}$, the

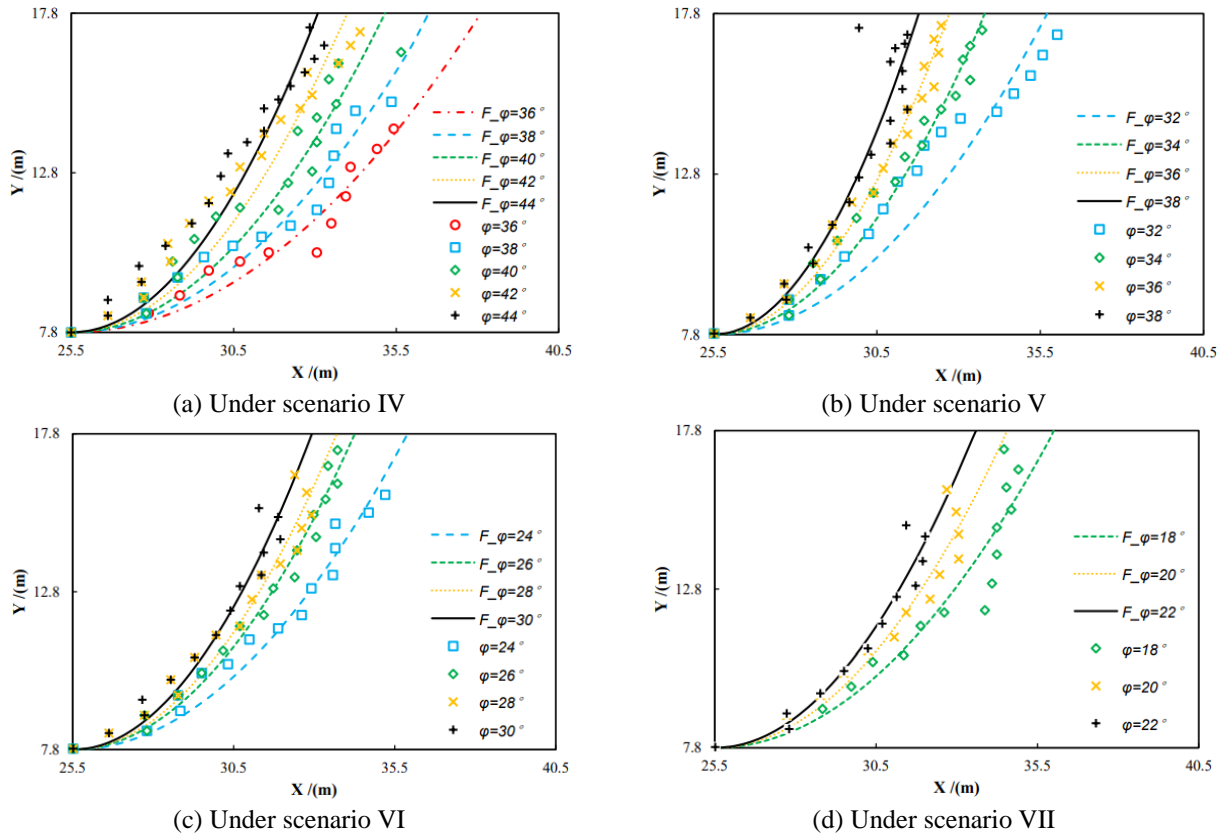


Fig. 4 Coordinates of key points on bottom boundary of plastic zone and their fit curves under different scenarios

sliding surface locates inside fillings, and when friction angle is larger than 44°, 38°, 30° or 22°, the sliding surface locates same as 44°, 38°, 30° or 22°, under the cohesion 1 KPa, 2 KPa, 3KPa or 4KPa, respectively, as illustrated in Table 3.

4. Location determining method for the critical sliding surface

4.1 Original sliding surface

The coordinates of key points on the bottom boundary of plastic zone are extracted and fitted by a parabola $y = f \cdot (x-25.5)^2 + 7.8$. Fig. 4 shows these coordinates of key points and their fit curves under scenarios (a) IV, (b) V, (c) VI and (d) VII, where the curve ‘ $F_{\varphi}=36^{\circ}$ ’ means the fit curve and the curve ‘ $\varphi=36^{\circ}$ ’ means coordinates of key points when φ is 36°. Values of the coefficient f are 0.0629, 0.0818, 0.1072, 0.1389 and 0.1736 when φ are 36°, 38°, 40°, 42° and 44° under scenario IV, are 0.0886, 0.0959, 0.1447 and 0.192 when φ are 32°, 34°, 36° and 38° under scenario V, are 0.0925, 0.1304, 0.1488 and 0.1811 when φ are 24°, 26°, 28° and 30° under scenario VI, and are 0.0903, 0.1217 and 0.1528 when φ are 18°, 20° and 22° under scenario VII, respectively. These fit curves are regarded as original sliding surface, and indicates that the original sliding surface becomes steeper with the internal friction angle as shown in Fig. 4.

4.2 Relation between the coefficient f and the friction angle φ

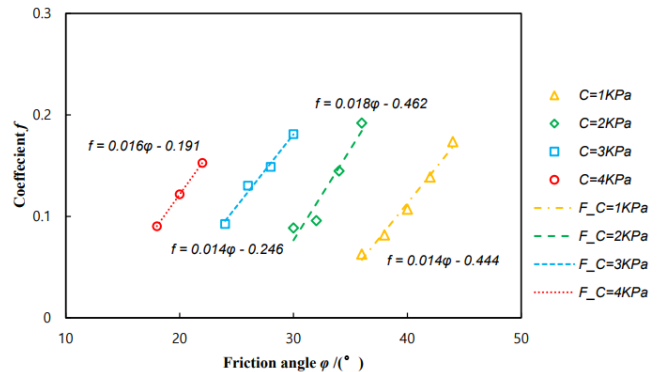


Fig. 5 Relation curves between the coefficient f and the friction angle φ under scenarios IV, V, VI and VII

Table 4 Fit relation curves between the coefficient f and the friction angle φ under different cohesions

Cohesion (KPa)	the Fit Curve of f - φ
1	$f = 0.014\varphi - 0.444$
2	$f = 0.018\varphi - 0.462$
3	$f = 0.014\varphi - 0.246$
4	$f = 0.016\varphi - 0.191$

Further research about the relation between the coefficient f and the friction angle φ is conducted. Relation curves between f and φ are obtained under scenarios IV, V, VI and VII as shown in Fig. 5, where the curve ‘ $C=1KPa$ ’ means values of f and the curve ‘ $F_C=1KPa$ ’ means the fit

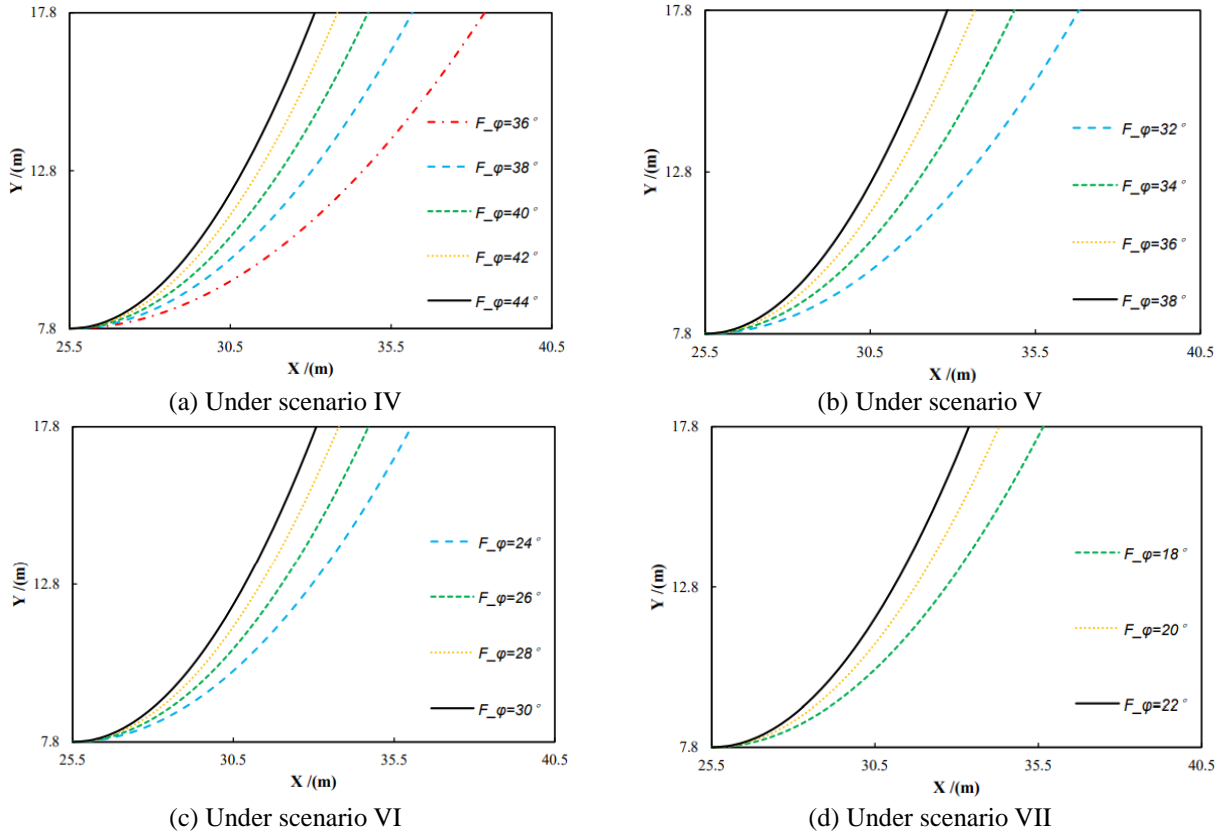


Fig. 6 Final sliding surface with different internal friction angles and cohesions

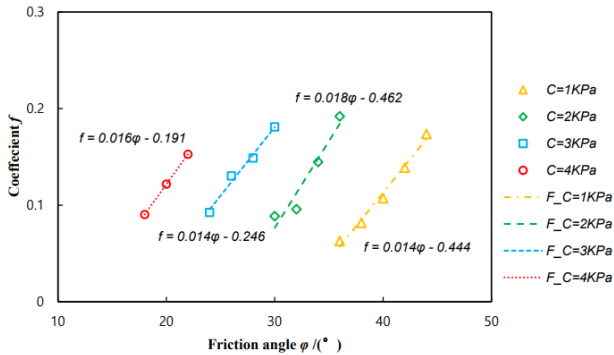


Fig. 7 Coordinates of key points on bottom boundary of plastic zone and their fit curves under different cohesions

relation curve when C is 1 KPa.

As seen from Fig. 5, the f increases approximately and linearly with the friction angle under the same cohesion. Fit relation curves between f and φ are $f = 0.014\varphi - 0.444$, $f = 0.018\varphi - 0.462$, $f = 0.014\varphi - 0.246$ and $f = 0.016\varphi - 0.191$, when C are 1 KPa, 2 KPa, 3 KPa and 4 KPa, respectively.

4.3 Final-determining of the sliding surface

The critical sliding surface can be determined by the fit relation curves, as illustrated in Table 4.

The final sliding surface for scenarios IV, V, VI and VII are drawn based on the fit curves of f - φ as shown in Fig. 6.

4.4 Influence of cohesion

Now that the sliding surface affected by cohesion, it is necessary to discuss the relation between the coefficient f and the cohesion C . Fig.7 shows coordinates of key points on bottom boundary of plastic zone and their fit curves under different cohesions 2.4 KPa, 2.6 KPa, 2.8 KPa and 3.0 KPa, and same friction angle 28°, where the curve ‘ $F_C=2.4KPa$ ’ means the fit curve and the curve ‘ $C=2.4KPa$ ’ means coordinates of key points when C is 2.4 KPa. Values of the coefficient f are 0.0807, 0.122, 0.1516 and 0.1488 when C are 2.4 KPa, 2.6 KPa, 2.8 KPa and 3.0 KPa, respectively. The original sliding surface becomes steeper with cohesion at first, but then the sliding surface under C 2.8 KPa is approximately same as that under C 3.0 KPa.

5. Conclusions

- Based on simulation results, a preliminary location of the sliding surface is determined. The sliding surface will locate on the bottom contact interface when the friction angle is relative small, such as smaller than 36°, 32°, 24° or 18° under the cohesion 1 KPa, 2 KPa, 3 KPa or 4 KPa, respectively. However, a weakened contact interface always becomes the critical sliding surface no matter what the friction angle is. In addition, when the critical sliding surface occurs inside fillings, potential slip objects extends up to the top of karst cave with a relative small cohesion, such as $C = 1$ KPa, but is confined to a small zone near the free face with a relative large cohesion, such as $C = 2$ KPa.

- The critical sliding surface will locate inside fillings when the friction angle becomes larger, such as larger than 36°, 32°, 24° or 18° under the cohesion 1 KPa, 2 KPa, 3 KPa or 4 KPa, respectively. The critical sliding surface can be determined by a parabola $y = f \cdot (x-25.5)^2 + 7.8$. The coefficient f increases linearly with the friction angle φ under the same cohesion, and is defined by $f = Q \varphi - P$. However, when friction angle is larger than 44°, 38°, 30° or 22°, the sliding surface locates same as 44°, 38°, 30° or 22° under the cohesion 1 KPa, 2 KPa, 3 KPa or 4 KPa, respectively.

- The critical sliding surface becomes steeper at first, but then remains unchanged approximately with cohesion under the same friction angle.

- Although affected by shape, size or position of the karst cave, the critical sliding surface mainly depends on both friction angle and cohesion. Thus, these research results and this method is always useful to determine the critical sliding surface. Of course, study on the influence of shape, size and position is need to be continued.

Acknowledgements

We appreciate the support from the National Natural Science Foundation of China (Grant No.: 51509147, 51879153), the Shandong Provincial Natural Science Foundation (Grant No.: ZR2018BEE045), the China Postdoctoral Science Foundation (2018M630780) and the Fundamental Research Funds of Shandong University (Grant No.s: 2017JC002, 2017JC001).

References

- Aliha, M.R.M., Ayatollahi, M.R., Smith, D.J. and Pavier, M.J. (2010), "Geometry and size effects on fracture trajectory in a limestone rock under mixed mode loading", *Eng. Fract. Mech.*, **77**(11), 2200-2212.
- Barpi, F., Barbero, M. and Peila, D. (2011), "Numerical modelling of ground-tunnel support interaction using bedded-beam-spring model with fuzzy parameters", *Gospodarka Surowcami Mineralnymi*, **27**, 71-87.
- Carrier, B. and Granet, S. (2012), "Numerical modeling of hydraulic fracture problem in permeable medium using cohesive zone model", *Eng. Fract. Mech.*, **79**, 312-328.
- Damjanac, B., Gil, I., Pierce, M., Sanchez, M., Van As, A. and McLennan, J. (2010), "A new approach to hydraulic fracturing modeling in naturally fractured reservoirs", *Proceedings of the 44th US Rock Mechanics Symposium and 5th US-Canada Rock Mechanics Symposium*, Salt Lake City, Utah, U.S.A., June.
- Gandomi, A.H., Kashani, A. R., Mousavi, M. and Jalalvandi, M. (2015), "Slope stability analyzing using recent swarm intelligence techniques", *Int. J. Numer. Anal. Meth. Geomech.*, **39**(3), 295-309.
- Gandomi, A.H. (2014), "Interior search algorithm (ISA): A novel approach for global optimization", *ISA Transact.*, **53**(4), 1168-1183.
- Guerriero, L., Coe, J.A., Revellino, P., Grelle, G., Pinto, F. and Guadagno, F.M. (2014), "Influence of slip-surface geometry on earth-flow deformation, Montaguto earth flow, southern Italy", *Geomorphology*, **219**, 285-305.
- Hajiazizi, M. and Taviana, H. (2013), "Determining three-

- dimensional non-spherical critical slip surface in earth slopes using an optimization method", *Eng. Geol.*, **153**, 114-124.
- Hoefsloot, F.J.M. (2008), "Analytical solution longitudinal behaviour tunnel lining", *Proceedings of the 6th International Symposium on Underground Construction in Soft Ground*, Shanghai, China, April.
- Kashani, A.R., Gandomi, A.H. and Mousavi, M. (2016), "Imperialistic competitive algorithm: A metaheuristic algorithm for locating the critical slip surface in 2-dimensional soil slopes", *Geosci. Front.*, **7**(1), 83-89.
- Khajehzadeh, M., Raihan Taha, M., El-Shafie, A. and Eslami, M. (2012a), "Locating the general failure surface of earth slope using particle swarm optimisation", *Civ. Eng. Environ. Syst.*, **29**(1), 41-57.
- Khajehzadeh, M., Taha, M. R., El-Shafie, A. and Eslami, M. (2011), "Search for critical failure surface in slope stability analysis by gravitational search algorithm", *Int. J. Phys. Sci.*, **6**(21), 5012-5021.
- Khajehzadeh, M., Taha, M.R., El-Shafie, A. and Eslami, M. (2012b), "A modified gravitational search algorithm for slope stability analysis", *Eng. Appl. Artif. Intel.*, **25**(8), 1589-1597.
- Khosravi, M. and Khabbazian, M. (2012), "Presentation of critical failure surface of slopes based on the finite element technique", *Proceedings of the GeoCongress 2012: State of the Art and Practice in Geotechnical Engineering*, Oakland, California, U.S.A., March.
- Li S.C., Lin P., Xu Z.H., Li, L.P., Guo, M., Sun, C.Q., Wang, J. and Song, S.G. (2015), "The minimum safety thickness of water and mud inrush induced by filled-type, karst water bearing structures based on the concept of slice method", *Rock Soil Mech.*, **7**, 1989-1994.
- Lin, P., Li, S.C., Xu, Z.H., Li, L.P., Huang, X. and He, S.J. (2016), "Analysis of stability of mud inrush induced by fillings sliding failure in karst cave based on the simplified Bishop Method and its application", *Proceedings of the Geo-China 2016: Emerging Technologies in Tunnel Engineering, Modeling, Design, Construction, Repair, and Rehabilitation*, Shandong, China, July.
- Mazaheri, A.R. (2015), "Use of line segments slip surface for optimized design of piles in stabilization of the earth slopes", *Int. J. Civ. Eng.*, **13**(1), 14-27.
- Metaya, S. and Bhattacharya, G. (2014), "Probabilistic critical slip surface for earth slopes based on the first order reliability method", *Indian Geotech. J.*, **44**(3), 329-340.
- Regmi, R.K. and Jung, K. (2016), "Application of dynamic programming to locate the critical failure surface in a rainfall induced slope failure problem", *KSCE J. Civ. Eng.*, **20**(1), 452-462.
- Rutqvist, J., Wu, Y.S., Tsang, C.F. and Bodvarsson, G. (2002), "A modeling approach for analysis of coupled multiphase fluid flow, heat transfer, and deformation in fractured porous rock", *Int. J. Rock Mech. Min. Sci.*, **39**(4), 429-442.
- Serdar, K., Tomas M., Fernandez, S. and Rafiq, A. (2015), "A numerical study on the Seepage failure by heave in sheeted excavation pits", *Geomech. Eng.*, **9**(4), 513-530.
- Yamin, M. and Liang, R.Y. (2010), "Limiting equilibrium method for slope/drilled shaft system", *Int. J. Numer. Anal. Meth. Geomech.*, **34**(10), 1063-1075.
- Yang, X.L. and Yan, R.M. (2015), "Collapse mechanism for deep tunnel subjected to seepage force in layered soils". *Geomech. Eng.*, **8**(5), 741-756.